

Transectional heat transfer in thermoregulating bigeye tuna (*Thunnus obesus*) – a 2D heat flux model

Jess Boye¹, Michael Musyl², Richard Brill^{3,*} and Hans Malte^{1,†}

¹Department of Zoophysiology, Institute of Biological Sciences, University of Aarhus, Denmark, ²Joint Institute for Marine and Atmospheric Research, Pelagic Fisheries Research Program, University of Hawaii at Manoa, Honolulu, HI 96822, USA and

³Cooperative Marine Education and Research Program, Northeast Fisheries Science Center, National Marine Fisheries Service, NOAA, Woods Hole, MA 02543, USA

*Present address: Virginia Institute of Marine Science, Gloucester Point, VA 23062, USA

†Author for correspondence (hans.malte@biology.au.dk)

Accepted 6 August 2009

SUMMARY

We developed a 2D heat flux model to elucidate routes and rates of heat transfer within bigeye tuna *Thunnus obesus* Lowe 1839 in both steady-state and time-dependent settings. In modeling the former situation, we adjusted the efficiencies of heat conservation in the red and the white muscle so as to make the output of the model agree as closely as possible with observed cross-sectional isotherms. In modeling the latter situation, we applied the heat exchanger efficiencies from the steady-state model to predict the distribution of temperature and heat fluxes in bigeye tuna during their extensive daily vertical excursions. The simulations yielded a close match to the data recorded in free-swimming fish and strongly point to the importance of the heat-producing and heat-conserving properties of the white muscle. The best correspondence between model output and observed data was obtained when the countercurrent heat exchangers in the blood flow pathways to the red and white muscle retained 99% and 96% (respectively) of the heat produced in these tissues. Our model confirms that the ability of bigeye tuna to maintain elevated muscle temperatures during their extensive daily vertical movements depends on their ability to rapidly modulate heating and cooling rates. This study shows that the differential cooling and heating rates could be fully accounted for by a mechanism where blood flow to the swimming muscles is either exclusively through the heat exchangers or completely shunted around them, depending on the ambient temperature relative to the body temperature. Our results therefore strongly suggest that such a mechanism is involved in the extensive physiological thermoregulatory abilities of endothermic bigeye tuna.

Key words: 2D model, archival tag, endothermy, isotherm, mathematical modeling, partial differential equation, temperature gradient, vascular countercurrent heat exchanger, white muscle, tuna.

INTRODUCTION

Tuna are highly specialized predatory fish with a unique assembly of anatomical, physiological and biochemical adaptations. Numerous studies have investigated these specializations such as fusiform body shape, thunniform swimming mode, capacity to conserve metabolic heat in red muscle, elevated metabolic and physiological rate functions, and a frequency-modulated cardiac output (Carey et al., 1984; Stevens and McLeese, 1984; Graham and Dickson, 2000; Lowe et al., 2000; Altringham and Shadwick, 2001; Brill and Bushnell, 2001; Gunn and Block, 2001; Katz et al., 2001; Sepulveda et al., 2003; Blank et al., 2004). In particular, the ability to conserve metabolically produced heat due to centralized red muscle and the presence of well-developed vascular countercurrent heat exchangers (also known as ‘retes’) has been thoroughly investigated (e.g. Carey et al., 1971; Mathieu-Costello et al., 1992; Block et al., 1993; Holland and Sibert, 1993; Dewar et al., 1994; Graham and Dickson, 2001; Korsmeyer and Dewar, 2001). Most attention has been focused on the heat exchangers associated with the red muscle fiber portions of the myotomes (herein referred to as ‘red muscle’). However, the white muscle fiber portions of the myotomes (herein referred to as ‘white muscle’) account for approximately 45–55% of total body mass (Graham et al., 1983; Freund, 1999) and the potential significance of the capacity of white muscle to produce and conserve heat remains largely unexplored.

A growing body of evidence confirms the ability of tuna to modulate muscle temperature by physiological thermoregulation or by a combination of physiological adjustments and behavior. This allows these fishes to appropriately adjust rates of body temperature change in the face of rapid ambient temperature changes induced by their extensive daily vertical excursions (Dewar et al., 1994; Graham and Dickson, 2001; Malte et al., 2007). It has been demonstrated that free-ranging bigeye tuna can change their whole-body thermal conductivity (as expressed by heating and cooling rates) by a factor of 100–1000 during vertical excursions (Holland and Sibert, 1993; Musyl et al., 2003). Modeling these observations in a two-compartment lumped parameter model further defined the ability of bigeye tuna to maintain elevated red muscle temperatures through behavioral and physiological means (Malte et al., 2007). The simple non-dimensional model described by Malte and colleagues (Malte et al., 2007) did not, however, distinguish between the different tissues in the tuna (the red muscle temperature referred to is just an overall elevated body temperature). Hence the model cannot reveal where in the body the heat is produced or conserved.

Carey and Teal (Carey and Teal, 1966) and Carey (Carey, 1973) confirmed the presence of an advanced countercurrent heat exchanger in red muscle when examining bigeye tuna, but they also describe, ‘...bands of alternate arteries and veins running into the light [i.e. white] muscle. These bands are widest and most numerous near the lateral vessels, where they may be 20 vessels

wide, but decrease to triads of artery–vein–artery toward the ventral and dorsal midlines'. The presence of a simple countercurrent heat exchanger in the white muscle reported in the early literature clearly provides evidence for the potential role of the white muscle in heat conservation and thermoregulation. We therefore decided to investigate the heat flux in different regions in the bigeye tuna. Because it is cumbersome to obtain direct measurements of the body temperature of tuna in motion (Dewar et al., 1994; Holland and Sibert, 1993), and because no experiment has so far elucidated the transsectional heat fluxes of any tuna, we decided to address these questions through mathematical modeling of heat flux. The questions we specifically addressed were: (1) does the white muscle contribute to the conservation of heat? (2) If so, is this conservation even noticeable? By developing a 2D model, we were able to simulate the heat flux and accurately predict temperature measurements made in free-swimming tuna, thereby acquiring a more profound understanding of the precise mechanisms responsible for the thermoregulatory abilities in this species. Our approach also enabled us to investigate a variety of features, including qualifying and quantifying the significance of the white muscle with respect to heat transfer and thermoregulation. We also determined the routes of heat loss, the possible extent of the modulation of heat transfer rates, and the role of body size.

MATERIALS AND METHODS

To explore the behavioral and physiological thermoregulatory capacities of bigeye tuna, two different models and related sets of data were required. (1) A steady-state model simulating the transsectional heat flux through the tuna's heat-producing tissues and heat-conserving modes. (2) A non-steady-state time-dependent model simulating the events associated with bigeye tuna's daily vertical movements. For the former we used data on isotherms in a cross-section of a bigeye tuna from Carey and Teal (Carey and Teal, 1966). For the latter we employed data on body temperature, water temperature and depth in free-ranging bigeye tuna from Musyl et al. (Musyl et al., 2003). In brief, Carey and Teal (Carey and Teal, 1966) caught bigeye tuna on long-line fishing gear during the winter of 1965–66 in the western North Atlantic and the eastern South Pacific. Once on board, the fish were sedated and the gills were perfused with sea water at low pressure while an irrigation system kept the fish at sea water temperature. For the next 3 h temperature measurements were made with thermistors. These probes were inserted into the muscle at a number of locations and isotherms were drawn by hand. Musyl et al. (Musyl et al., 2003) captured 87 bigeye tuna by conventional long-line gear and by rod and reel near the main Hawaiian Islands from April 1998 to April 2001. On board Wildlife Computers (Redmond, WA, USA) archival tags were implanted through a 1–1.5 cm incision into the peritoneal cavity and placed approximately as illustrated by the black circle in Fig. 1B. The tags sampled data on four channels every 60 s: depth, light, internal and external temperature. Post-operatively the fish were released and the data were downloaded from the tags from recaptured tuna.

Modeling

To analyze the cross-sectional isotherms and the time-dependent temperature changes, we developed a 2D heat flux model of a cross-section of a bigeye tuna. The model included the following assumptions.

(1) The thermal properties of tissues/organs (muscle, bone, gut, etc.) differ but are identical everywhere within any tissue/organ.

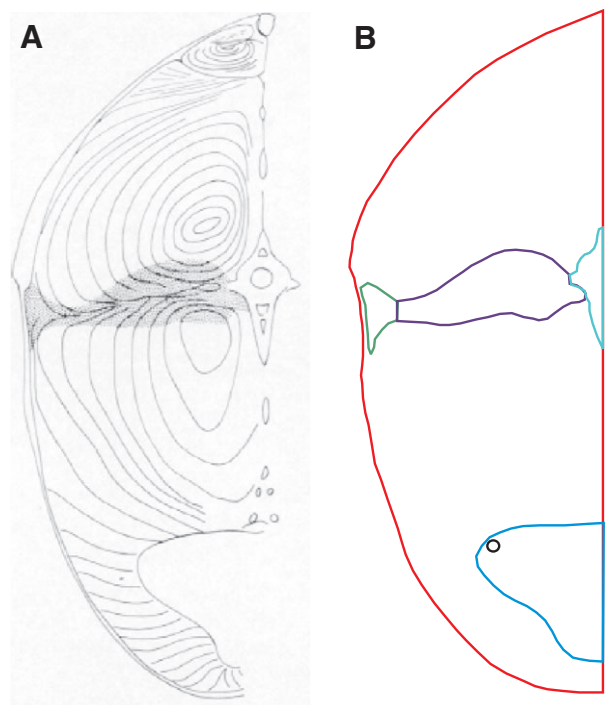


Fig. 1. The real cross-section of the bigeye tuna (A) and the modeled cross-section (B) showing the outline of the different domains: red muscle (purple), white muscle (red), gut (blue), rete (green), temperature sensor (black) and bone (cyan).

- (2) The given cross-section is representative for the entire tuna [i.e. the tuna is 'infinite' in length (the z -coordinate) and does not alter shape].
- (3) There is a non-directional, uniform convective heat transfer to the environment by the blood. This heat transfer is modified by the presence of vascular heat exchangers.
- (4) There is no significant thermal boundary layer and the skin temperature is uniform and everywhere equal to the ambient water temperature.
- (5) The heat flux of the cross-section is symmetrical across the vertical axis of the tuna (i.e. the net heat flux across this symmetry line is zero).
- (6) All energy liberated in metabolism is eventually converted into heat.

Heat dissipation through the tuna (and thus through the cross-section) follows Fourier's law of heat conduction. This results in a second-order partial differential equation:

$$\frac{\partial T_b}{\partial t} = \nabla \cdot (\kappa \nabla T_b) + \dot{T}_p - \varphi (T_b - T_w)(1 - \varepsilon) \quad (1)$$

The last term in Eqn 1 holds for the 2D homogeneous case with constant thermal diffusivity. Inclusion of the metabolic heat produced within the body of the tuna and the convective loss by the blood, which is cooled in the gills, yields the following equation:

$$\frac{\partial T_b}{\partial t} = \nabla \cdot (\kappa \nabla T_b) + \dot{T}_p - \varphi (T_b - T_w)(1 - \varepsilon) \quad (2)$$

where \dot{T}_p is temperature production, i.e. the rate of change in temperature due to heat production ($^{\circ}\text{C s}^{-1}$, see Appendix), T_b is body temperature at a given coordinate ($^{\circ}\text{C}$), T_w is water temperature ($^{\circ}\text{C}$), $\kappa = K/(pc_p)$ is thermal diffusivity ($\text{cm}^2 \text{s}^{-1}$), K is thermal

conductivity ($\text{J s}^{-1} \text{cm}^{-1} \text{C}^{-1}$), ρ is density (g cm^{-3}), c_p is specific heat capacity ($\text{J g}^{-1} \text{C}^{-1}$), $\beta = \rho c_p$ is the heat capacitance coefficient ($\text{J cm}^{-3} \text{C}^{-1}$), ε is heat exchanger efficiency (dimensionless), $\varphi = \dot{v}_b (\beta_{\text{blood}} / \beta_{\text{muscle}})$ is the convective cooling rate constant (s^{-1}), \dot{v}_b is specific blood flow ($\text{cm}^3 \text{blood s}^{-1} \text{cm}^{-3} \text{muscle}$), t is time, ∇ is the gradient operator, $\nabla \cdot$ is the divergence operator. A derivation of the equation and a more detailed account of the meaning of the operators and the different terms are given in the Appendix.

Because second-order non-linear partial differential equations are virtually impossible to solve analytically, this was accomplished *via* numerical analysis by the methods of finite elements using the commercial software package FlexPDE® (PDE Solutions, Inc., CA, USA).

The steady-state model

At a sea water temperature of 20°C (T_w), the 70 kg bigeye tuna presented in Carey and Teal (Carey and Teal, 1966) had a body temperature (T_b) of 32°C in the center of the red muscle. The highest T_b was found deep in the lateral muscle behind the pectoral fin, which is the thickest part of the fish. We developed a model to predict the isotherms of the cross-section of this fish.

We estimated body depth (the vertical distance, i.e. height of the fish in a transection at the thickest part of the body) relative to fork length and body mass by applying a geometric model of tuna body shape developed by Magnuson and Weininger (Magnuson and Weininger, 1978). We calculated fork length to be 144 cm (based on the relationship between body mass (M) and fork length (L) in bigeye tuna: $M=0.00961L^{3.18}$) and body depth to be 42.8 cm. Once the scale was in place, the construction of the shape of the cross-

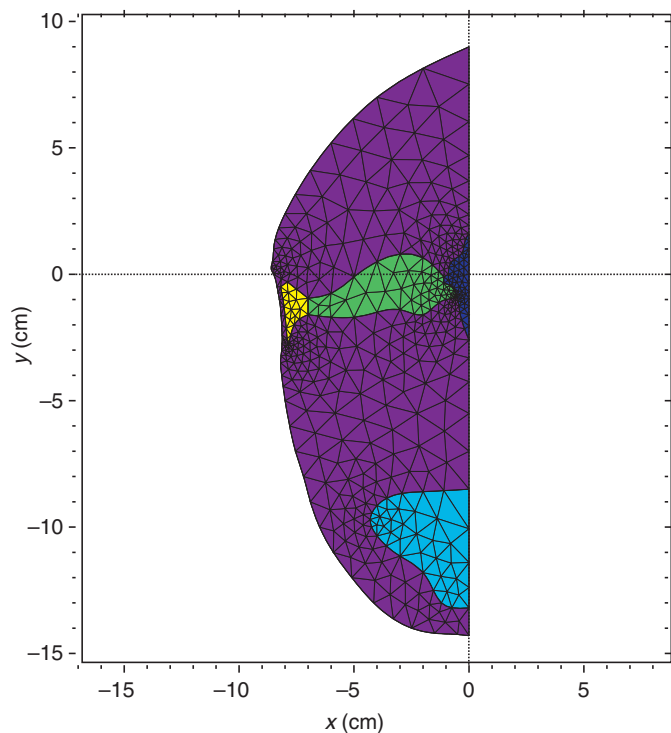


Fig. 2. An example of a rough mesh grid of the entire cross-section. The density of the mesh depends on the required accuracy of the calculations. The mesh will automatically adapt as calculations proceed in order to keep the error below a set limit. The final mesh will typically be of higher density than shown here.

section was accomplished using a spline function. To account for all thermally conductive regions of the body, the respective domains were implemented in the model (Fig. 1) and boundary conditions were specified. Each region was assigned a specific thermal property (Table 1). In a highly vascularized tissue such as the red muscle the natural convective fluctuations in the xy -coordinate direction due to blood flow could be expected to increase the effective thermal diffusivity, κ . However, experiments on tissue thermal conductivity performed on rats indicated that the contribution of blood flow to thermal diffusivity is negligible (Song et al., 1999; Cheng et al., 2002).

The volume-specific heat production in muscle was determined from the maximum oxygen consumption ($\dot{V}_{O_2\text{max}}$), 2700 mg O₂ kg⁻¹ h⁻¹ (Bushnell and Brill, 1991; Dewar and Graham, 1994), assuming all the energy extracted from the oxygen is eventually converted into metabolic heat (i.e. $\dot{h}_p = \dot{V}_{O_2} \times$ calorific coefficient of O₂). The maximum metabolic rate was selected in order to assess the maximal heat production, thus setting the lower limit for the estimated heat exchanger efficiencies. The volume-specific heat production in the red and white muscle was calculated from the average heat production and the relative area contributions of the two types of muscle by assuming their ratio was equal to the ratio of capillarity in the respective tissues (5.3≈2880 mm⁻²/543 mm⁻²) (from Mathieu-Costello et al., 1992). The specific blood flow in the convective cooling rate constant was calculated from:

$$\dot{v}_b = \frac{\dot{V}_{O_2}}{\rho \Delta S \times O_2 \text{ carrying capacity}} . \quad (3)$$

The oxygen-carrying capacity was set at 0.16 ml O₂ cm⁻³ blood (Malte et al., 2007). The saturation difference between oxygenated and deoxygenated blood (arterial and venous blood) was set at $\Delta S=0.5$. When solving Eqn 2, FlexPDE® utilized the finite element method of separating the domain in question into mesh grids of lengths that are finitely minute. This resulted in a linear approximation of the partial differential equation until a pre-selected margin of error was reached (Fig. 2).

To solve the heat transfer problem at steady state, Eqn 2 must equal zero. That is:

$$\nabla \cdot (\kappa \nabla T_b) + \dot{T}_p - \varphi (T_b - T_w) (1 - \varepsilon) = \frac{\partial T_b}{\partial t} = 0 . \quad (4)$$

Because of symmetry, only half the cross-section of the tuna was modeled by applying a boundary condition of zero heat flux across the line of symmetry (i.e. $\partial T_b / \partial n = 0$, where n is the normal to the surface). On the rest of the boundary the condition $T_b = T_w$ was applied. By definition, the term in Eqn 4 will only approach zero at a given accuracy and an error limit was set at 1×10^{-6} for all calculations.

To simulate the observed isotherms obtained by Carey and Teal (Carey and Teal, 1966) at 20°C T_w , a reasonable heat exchanger efficiency value had to be estimated for both the red and white

Table 1. Thermal properties applied in the model

	Water	Muscle	Bone
κ (cm ² s ⁻¹)	1.45×10^{-3} ^a	1.11×10^{-3} ^b	9.64×10^{-4} ^c
c_p (J g ⁻¹ °C ⁻¹)	4.179 ^a	3.52 ^f	3.0506 ^c
ρ (g cm ⁻³)	0.9974 ^a	1.06 ^d	1.00 ^e

The gut region was assigned values as water. ^aHolman, 1989 (at 21.22°C).

^bHensel and Bock, 1955. ^cCaltenburg et al., 2004. ^dUrbanchek et al., 2001. ^eBonnick, 2000. ^fNgadi and Ikediala, 1998.

muscle. The estimated value was considered satisfactory if the modeled isotherms closely resembled the experimentally determined isotherms.

The time-dependent model

Bigeye tuna descend at dawn to depths of 300–500 m and make regular upward excursions into the warmer surface layer, then ascend at dusk to remain at the surface layer until the following dawn (Musyl et al., 2003). The upward excursions are made in order to warm the body rapidly. The fish then descends while retaining the newly gained heat. Fish 241 (from Musyl et al., 2003) was selected because it clearly demonstrated this vertical movement pattern characteristic of bigeye tuna (Fig. 3).

The non-steady-state model was based on a modification of the steady-state model. The time dependency relied on the fact that T_w (and therefore also T_b) varies in time as the tuna descends and ascends, thus altering the model into a non-steady-state problem. The processed external (T_w) temperature data from the archival tag of Fish 241 were imported into the model and these were used in Eqn 2 so that $T_w = T_w(t)$ during its solution. The shape of the 2D cross-section of the bigeye tuna was set as identical to the steady-state model, but the dimensions were resized to fit the physical proportions of Fish 241. The calculations on the new dimensions were based on the formerly presented geometric model. Fish 241 had a fork length of 79 cm and a body mass of 10.3 kg, yielding a modeled body depth and body mass of 23.5 cm and 10.4 kg, respectively. The model was designed to allow for scaling with the placement of the internal organs preserved. A sensor region was introduced to the model to simulate the actual sensor position of

the archival tag. As in Musyl et al. (Musyl et al., 2003) it was placed in the visceral cavity (Figs 1 and 2) and given an equivalent dimension.

An imitated shunt mechanism was implemented to allow for active thermoregulation. The shunt mechanism was assumed to direct the blood flow either: (1) through the countercurrent heat exchangers (hence conserving metabolically produced heat) or (2) around the countercurrent heat exchangers (possibly by passing the blood through the dorsal aorta and post-cardinal vein). This is a plausible route of active thermoregulation in the bigeye tuna as suggested by Malte et al. (Malte et al., 2007). We chose to use only the simplest possible mode of thermoregulation: either all the blood flow is through the exchanger or all the blood is bypassing the exchanger. This was achieved in the model by letting the efficiency (ε) of the heat exchanger vary according to:

$$\varepsilon = \varepsilon_{\text{fit}} (1 - f), \quad (5)$$

where ε_{fit} is the heat exchanger efficiency fitted from the steady-state model and f is the fraction of blood bypassing the rete. The shunt fraction is then varied according to:

$$f = \begin{cases} f_{\text{high}} & \text{for } T_w - T_b > 0 \\ f_{\text{low}} & \text{for } T_w - T_b < 0 \end{cases}. \quad (6)$$

Thus ε in Eqn 5 attains a high value whenever $T_w < T_b$, and a low value whenever $T_w > T_b$. The oxygen consumption was assumed to have either of two values – a ‘resting’ and an active value (i.e. a two-state diurnal metabolism). When in nocturnal swimming mode, the bigeye tuna display a reduced vertical swimming activity,

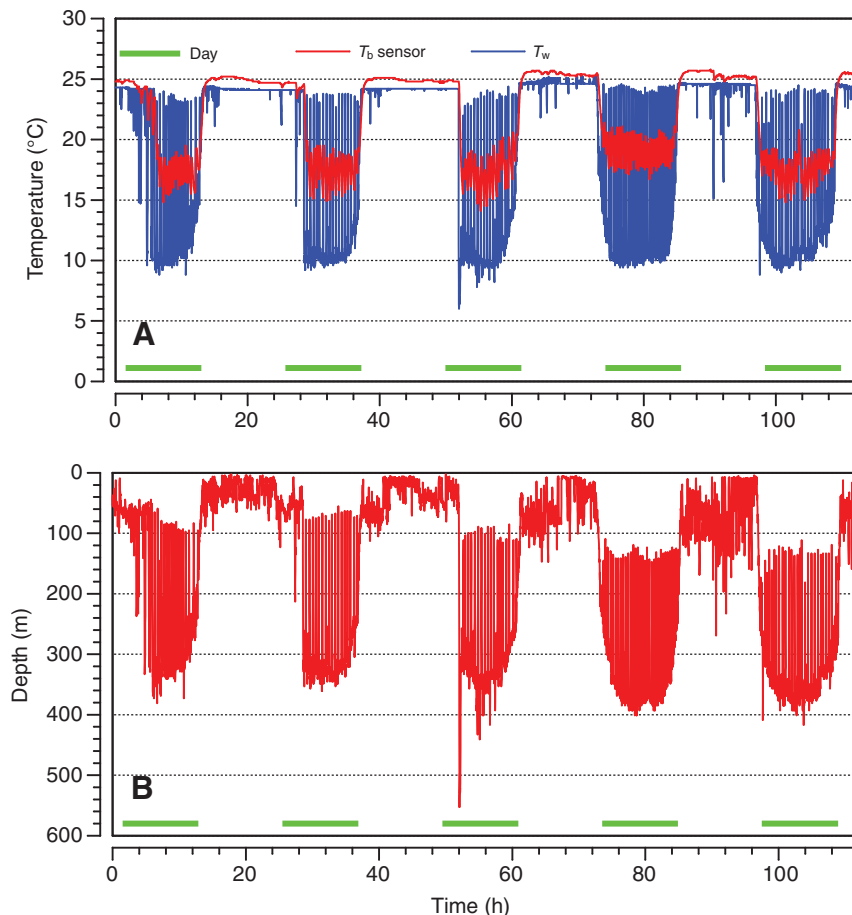


Fig. 3. A representative time segment of daily excursions of Fish 241. (A) Water (T_w) and sensor (T_b sensor) temperature records. (B) The characteristic W-shaped vertical movement patterns of bigeye tuna during the daytime.

therefore referred to here as ‘resting’. They swim in the horizontal plan, possibly to catch prey, while maintaining the minimum speed required to ram ventilate and avoid sinking. At dawn, the fish enters an active swimming mode, descending to greater depths and then either feeding or swimming to the surface and down again, increasing its oxygen consumption. Calculations of the vertical swimming speed based on the depth data exhibited a clear consistency with the assumption of low cruising mode at night with low swimming speeds, and an active swimming mode during the day with high swimming speeds (Fig. 3). Hence the shift in oxygen consumption was modeled based on the day/night cycle, simply as:

$$\dot{V}_{O_2}(x) = \begin{cases} \dot{V}_{O_2\text{max}} & \text{for } x=1 \\ \dot{V}_{O_2\text{rest}} & \text{for } x=0 \end{cases}, \quad (7)$$

where x is an array in which daytime is given the number 1 and 0 is for night-time. $\dot{V}_{O_2\text{rest}}$ was set at a routine metabolic rate of $540 \text{ mg O}_2 \text{ kg}^{-1} \text{ h}^{-1}$ (Freund, 1999). Thermal properties, heat production h_p and the fitted heat-conserving efficiency (ϵ_{fit}) for red and white muscle from the steady-state model were applied. The model was considered satisfactory if it predicted values of T_b at the sensor region that intimately followed the T_b values recorded by the sensor tag and the adjusted parameter was now the shunt fraction (Eqn 5).

RESULTS

Fig. 4 illustrates cross-sections of the recorded isotherms (Fig. 4A) and the isotherms predicted by the model (Fig. 4B). It is obvious that the observed and predicted results match and that the model simulates the 2D heat flux in the fish quite well. The highest temperatures are in the heat-generating red muscle from which there is a heat flux down the thermal gradient into the adjacent white

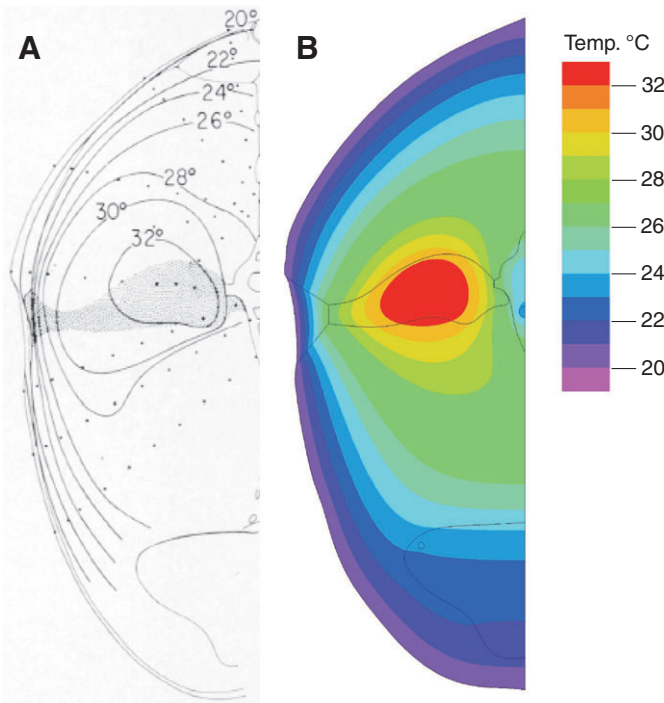


Fig. 4. Plots of the isotherms in the bigeye tuna. (A) The thermal distribution as observed by Carey and Teal (Carey and Teal, 1966). The isotherms are hand drawn and estimated on the basis of thermistor readings (black dots in the figure). (B) The simulated temperature distributions and isotherms.

muscle. A fraction of the heat flux will pass through the gut and finally reach the surface of the bigeye tuna in contact with 20°C sea water. The best match, as shown in the figure, was obtained when the efficiency of the heat exchangers supplying blood to the red and white muscle was 99% and 96%, respectively.

To better display the precision of our estimates, Fig. 5 shows the temperature profile along the secant line through the isotherms of the cross-section illustrated in Fig. 4B. This specific cross-section includes all observed isotherms traversing the point of maximal temperature in the red muscle (Fig. 5C). Fig. 5A displays the

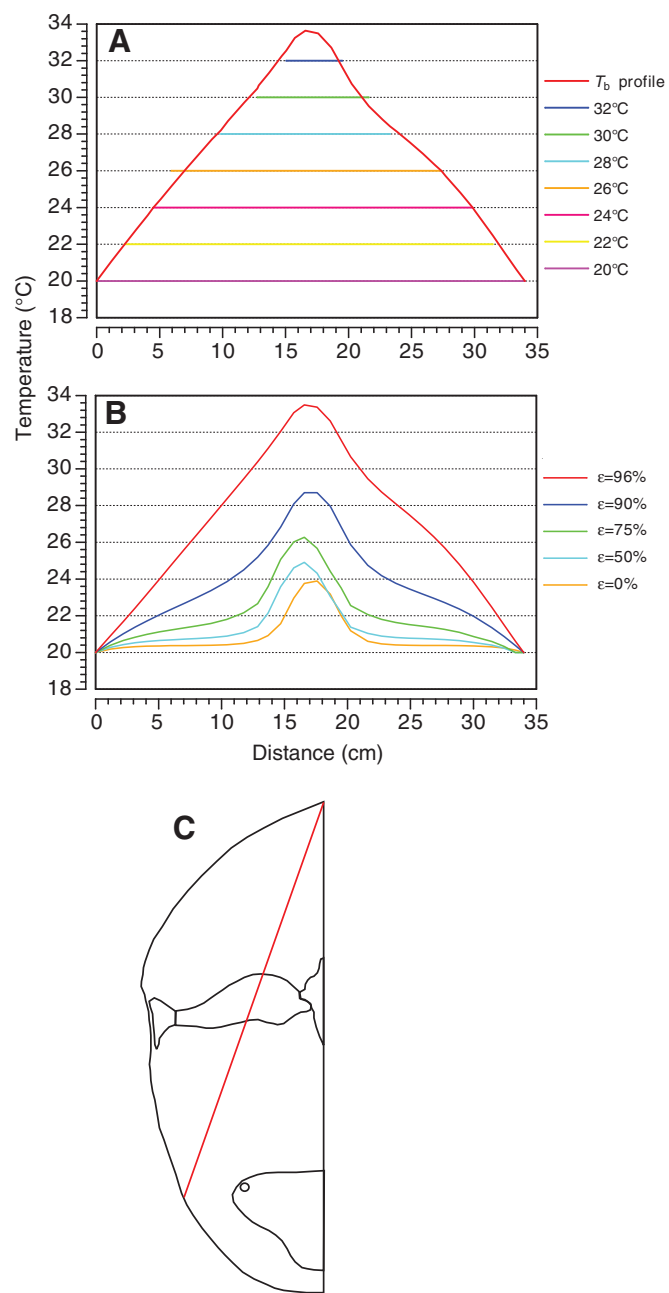


Fig. 5. Introducing a secant line intersecting the cross-section of the tuna (C) generates a 1D body temperature profile (A) from the simulated heat transfer in Fig. 4B depicted with an identical secant line traversing the measured isotherms in Fig. 4A. B illustrates the effect of a reduced white muscle rate efficiency on this 1D temperature profile. Notice the profound effect of reducing rate efficiency from 96 to 90%.

smoothly fitting curvature of the predicted body temperature profile and the isotherms recorded by Carey and Teal (Carey and Teal, 1966). This close fit was only achieved using the above-mentioned heat exchanger efficiencies. The deviations of the modeled T_b profile are not considerably different from the observed isotherms, when disregarding the outlier at the 26°C isotherm. Fig. 5B shows the significance of a high degree of heat conservation in the white muscle. It is clear that only at $\epsilon_{\text{white}}=96\%$ is it possible to recreate the observed isotherms (ϵ_{red} being fixed at 99%), thus stressing the importance of heat conservation in the white muscle. The impact of the high efficiency rete in the blood supply to the white muscle can be seen when comparing the 90% curve (blue) and 96% curve (red). The integrated area under the 96% curve is almost twice as large ($235/125=1.88$) as the area under the 90% curve.

To further explore the consequence of an absence of a rete in the blood supply to the white muscle ($\epsilon_{\text{white}}=0\%$), we plotted the temperature distribution in the 2D cross-section (Fig. 6). The temperature distribution is very different from that in Fig. 4B. Any heat produced in the white muscle will rapidly be lost *via* the convective blood flow resulting in 'lumps' of isotherms at the boundary of the red muscle. Even though the efficiency of the rete in the red muscle is maintained at 99%, the warmest point is only 26°C as opposed to 32°C in Fig. 4. We thus conclude that the high temperatures and isothermal distribution observed by Carey and Teal (Carey and Teal, 1966) require the presence of an effective countercurrent heat exchanger in the vascular system supplying blood to white muscle.

To quantify the loss of heat across the surface of the fish, the heat flux vectors (Fig. 7A) at the periphery were integrated (Fig. 7B). This yielded a surface heat loss of $0.622 \text{ J s}^{-1} \text{ cm}^{-1}$ at a total heat

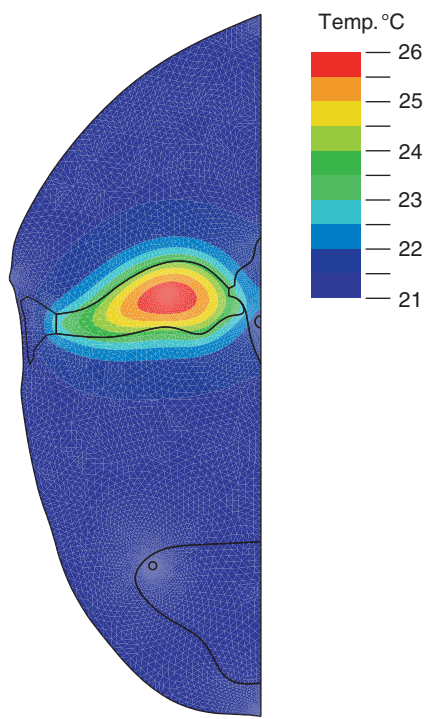


Fig. 6. The modeled temperature distribution obtained when heat conservation in the white muscle is turned off (rete efficiency=0). Note the steep temperature gradient at the border between red and white muscle. Maximum red muscle temperature is 26°C, compared with 32°C in Fig. 4.

production of $1.886 \text{ Js}^{-1} \text{ cm}^{-1}$ (i.e. surface heat loss accounts for approximately 33% of total heat production). Despite the relatively high efficiencies of the vascular countercurrent heat exchanger ($\epsilon_{\text{red}}=99\%$, $\epsilon_{\text{white}}=96\%$), approximately two-thirds of the heat produced is still lost *via* the gills. If ϵ_{red} and ϵ_{white} were 100%, all the heat produced would have to be lost across the surface. When testing this notion in the model, we found a 99.6% surface heat loss, thus confirming the suitability of our methods.

The mass to heat loss relationship was modeled to determine the significance of body size. This was accomplished *via* the scalability of the modeled cross-section of the bigeye tuna. The relationship between mass and surface heat loss:total heat production ratio is

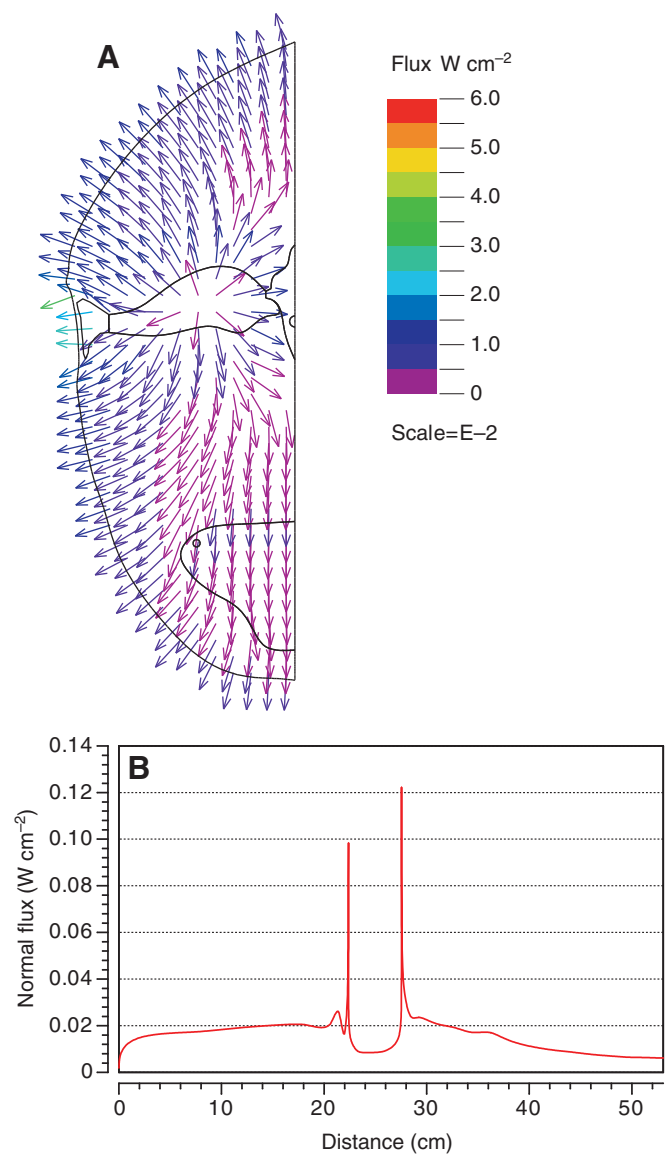


Fig. 7. Heat loss across the surface of the fish represented as heat flux vectors (A). The lengths of the flux vectors are normalized and their magnitudes are represented by color. Note that the net flux across the symmetry line is zero. (B) The magnitude of the normal (perpendicular to the surface) flux as a function of distance along the boundary from top to bottom. The area under this curve is the total heat loss per cm of depth. Note that the two sharp peaks are artifacts that arise in the numerical calculations because of the sharp edges in the geometry here. They do not contribute to the area under the curve.

presented in Fig. 8 (blue curve). The hyperbolic shape of the curve is expected because of the surface to volume ratio (i.e. small fish have larger relative surface areas than larger fish). At a mass of approximately 7 kg, 50% of the heat production is lost *via* convection through the blood and 50% *via* conduction through the skin. In order to investigate the implication of an increased body size on the temperature in the warmest area of the body, the relationship between maximal T_b in the red muscle and mass was established (red curve in Fig. 8). The curve in the logarithmic plot is sigmoid and appears to converge to a limit [data not shown at an unrealistically high body mass: bigeye tuna 170.6 kg, bluefin tuna (*Thunnus thynnus*) 678.6 kg; <http://www.bigmarinefish.com>]. The curve fits well with the mass and temperature of the red muscle of the steady-state model. Additionally, the curve fits with isotherms in cross-sections of smaller fish throughout the body of the tuna examined by Carey and Teal (Carey and Teal, 1966) (data not shown). A 1 kg fish would have a sustained T_x (maximal temperature elevation compared with the ambient water) of approximately 3.5°C, and a sustained T_x of 10°C required a mass of approximately 20 kg.

We used the archival tag data for a selected daytime period of Fish 241 of Musyl et al. (Musyl et al., 2003) to test the time-dependent model. The specific day was chosen based on the criterion that it was representative of the bigeye tuna behavioral swimming pattern (i.e. regular excursions in between the uniform-temperature surface layer and depths at approximately 350 m such as day 4 in Fig. 3). A typical example of water temperature, recorded body temperature, and modeled body temperature during the daytime for Fish 241 is displayed in Fig. 9A. T_w rapidly

decreased as the fish descended, while T_b decreased much more slowly. For each excursion to the uniform-temperature surface layer, there was a rapid increase in T_b accompanied by a slow decrease when returning to depth. This difference in heating and cooling rate considerably magnified the average difference between T_w and T_b . The average T_b is approximately 19.3°C during the regular excursions. However, the range of T_b during the regular excursions (approximately 17–22°C) is far more interesting. The tuna seems tolerant of a reduction in T_b to only 17°C. When T_b reached this value the tuna initiated the rapid ascent to warmer surface waters. Likewise, when T_b reached about 22°C, the fish commenced its descent. The modeled T_b which, for this purpose, was the average temperature of the sensor region in the geometry (Fig. 1), follows the recorded T_b remarkably well and only during the last three excursions does a minor, but noticeable, discrepancy develop. This close fit was achieved by letting the shunting fraction (f) vary simply between 0 and 1 (i.e. all the blood either passed through the heat exchangers or completely bypassed it; Eqn 5). Since Fish 241 used for the time-dependent model was somewhat smaller than the tuna used for the steady-state model, the efficiency of the heat exchanger supplying blood to the red muscle had to be increased from 99% to 99.5% to reproduce measured T_b values. The precision of the fit can be better appreciated in Fig. 9B, which shows an expanded segment of Fig. 9A. This figure reveals that rapid modification of the heating and cooling rates (physiological thermoregulation) can be achieved by shunting blood through or around the heat exchanger resulting in a significant degree of control over T_b . When preventing physiological thermoregulation by holding the parameters f and ϵ constant, the modeled T_b did not in any way resemble the measured T_b values (data not shown). This re-emphasizes similar findings previously obtained by Holland and Sibert (Holland and Sibert, 1993) and Malte et al. (Malte et al., 2007). We tested the effects of pure thermal inertia in the time-dependent model by scaling up the geometry, reducing the efficiency of the rete, and lowering the oxygen consumption; thus simulating a large ectothermic teleost. The result was a curve radically different from the simulations derived from modeling a thermoregulating bigeye tuna. In the model simulating a large ectothermic teleost, T_b follows T_w when the fish resides in the surface layer. However, when the fish descends into colder water, T_b follows T_w but with a noticeable delay. Similarly when the fish ascends there is a delay in T_b since the thermal inertia works both ways. However, even with frequent regular vertical excursions, the virtual ectotherm maintained a T_x of only 2°C (data not shown).

DISCUSSION

Steady-state heat exchange

It has been assumed that white muscle is warmed *via* conduction from the deep red muscle (Korsmeyer and Dewar, 2001). Based on our results, however, this appears not to be entirely correct. When we set the parameters in our model to assume that there is no rete in the vascular system supplying blood to the white muscle (i.e. zero rete efficiency and that the white muscle is warmed solely by heat conducted from the red muscle), the model does not predict the isotherms reported by Carey and Teal (Carey and Teal, 1966) (Fig. 6). Moreover, not even when setting $\epsilon_{\text{red}}=99.999\%$ could we reproduce the recorded temperatures when $\epsilon_{\text{white}}=0$. Only when multiplying the maximal metabolic rate by at least a factor 10 is it possible to reach red muscle temperatures 12°C above T_w .

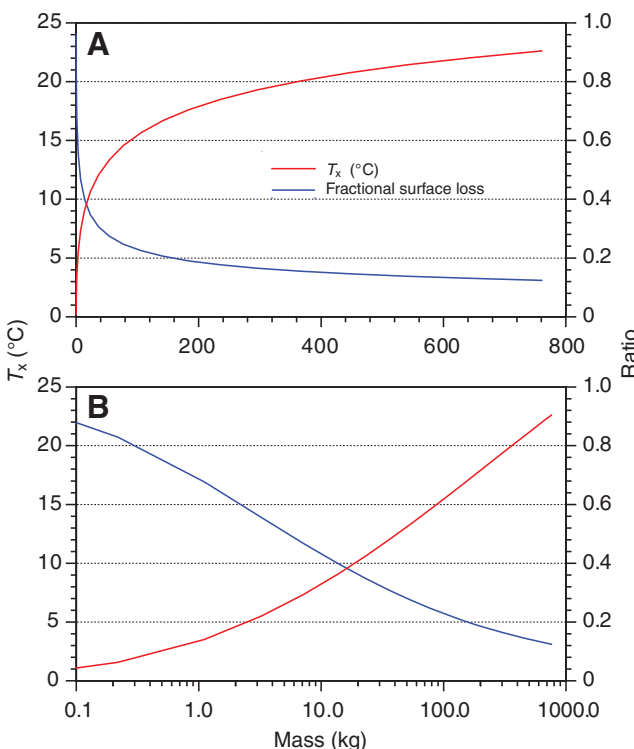


Fig. 8. The modeled relationship between body mass and the surface heat loss:total heat production ratio (blue curve), and the maximal temperature elevation in the red muscle compared with the ambient water at 20°C (T_x ; red curve). Volume-specific oxygen consumption and rete efficiencies were held constant. (A) Linear x-axis. (B) Logarithmic x-axis.

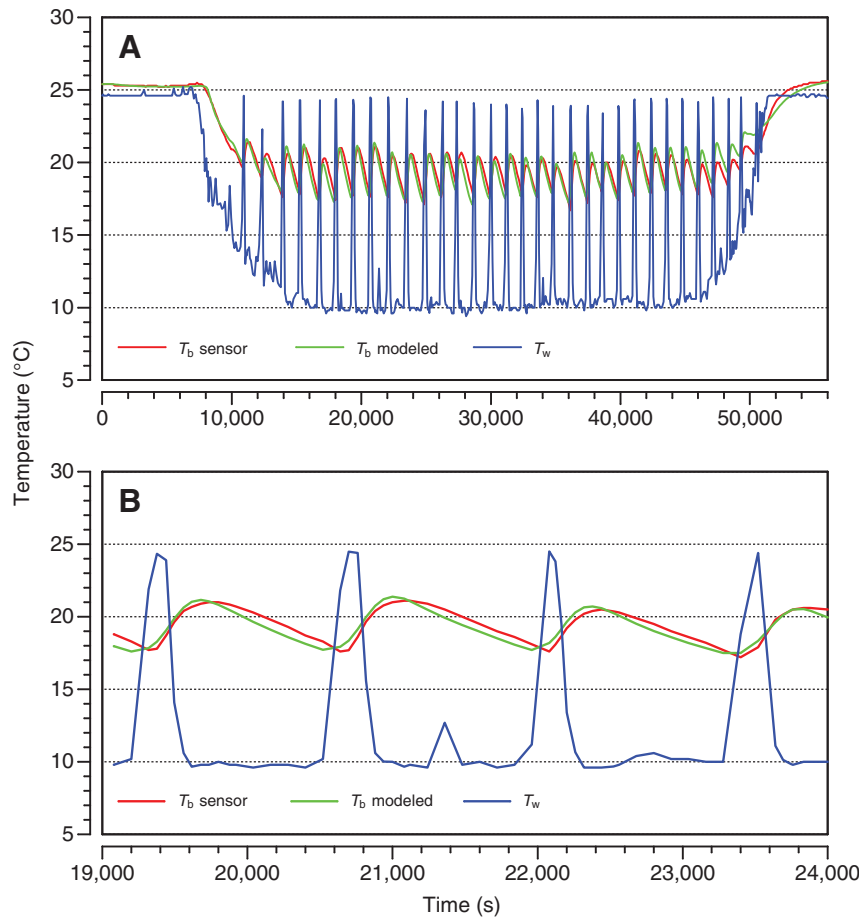


Fig. 9. (A) Temperature records from the sensor in the water (T_w) and the sensor in the body (T_b sensor) during a typical daytime period for Fish 241, along with the simulated body temperature at the sensor location (T_b modeled). This temperature was the averaged temperature over the sensor region. (B) An expanded segment of A reveals the close agreement between the measured and the modeled temperature during four vertical excursions.

Rather, our model shows that: the presence of a functional rete in the blood supply to the white muscle is necessary to achieve realistic model outputs, less than 33% of the heat produced by the red muscle is actually conducted to the white muscle, and the white muscle is warm primarily because of the heat that it itself produces, as well as the heat it receives from the red muscle. Moreover, the white muscle aids temperature elevation in the red muscle by exerting an insulating effect (i.e. lowering the thermal gradient between the red and white muscle) (Figs 4 and 6). The heat-conserving capacity of the white muscle therefore not only serves to elevate the metabolic activity of this tissue but also provides the potential for the red muscle to reach the high temperatures that Carey and Teal (Carey and Teal, 1966) recorded. The parameter ΔS (oxygen saturation difference between arterial and venous blood) was set at a value of 0.5. It could be argued that the ΔS in the muscle is higher during elevated swimming speeds. However, setting $\Delta S=1$ yielded only a minor reduction in heat exchanger efficiency ($\varepsilon_{\text{red}}=97\%$ and $\varepsilon_{\text{white}}=94\%$) compared with when $\Delta S=0.5$.

The vascular countercurrent heat exchangers in the red muscle are indeed well developed with 4-to-1 modules arranged in tight compaction (Stevens et al., 1974). However, Carey and Teal (Carey and Teal, 1966) described the rete in the white muscle as vascular bands near the skin surface which ultimately split up in triads in the deep muscle. Considering the clearly simpler construction of the rete in the blood supply to the white muscle, the $\varepsilon_{\text{white}}=96\%$ implied by the results of our calculations seems surprising. Preliminary simulations of heat fluxes in different rete arrangements, however, indicate that this is indeed possible

(H.M., in preparation). Nevertheless, the vascular countercurrent heat exchanger in the red muscle still conserves heat four times better than the simpler triad heat exchanger in the white muscle (the factor $1-\varepsilon$ in Eqn 2).

Because of the larger mass of the white muscle, total heat production within this tissue is approximately 2.3 times larger than that in the red muscle. The ratio of red and white muscle mass to total body mass is 6–9% and 45–55%, respectively (Graham et al., 1983; Freund, 1999). Integrating the muscle mass in relation to the total body mass in the specific cross-section in our model yields a relative red and white muscle mass of 6.6% and 82.2%, respectively. The modeled cross-section is located just behind the pectoral fin, the thickest part of the fish, whereas the 45–55% is an expression of the total white muscle mass in all three dimensions. This explains the discrepancy in the fraction of white muscle mass.

The finding of the white muscle as a significant contributor in heat conservation is also relevant to the evolution of endothermy in fish. Our results suggest that the rete in the blood supply to the white muscle most likely evolved either simultaneously with, or before, the rete in the blood supply to the red muscle and the internalization of the red muscle. If it had not, our results clearly imply that internalization of the red muscle alone would not allow significant sustained temperature elevation of the red muscle without the presence of a rete in the blood supply to the white muscle.

The time-dependent setting

In the time-dependent model, the assumed blood flow patterns were either that all the blood went through the rete to conserve metabolically

produced heat (when $T_b > T_w$) or all the blood bypassed the rete (when $T_w > T_b$). Likewise, the oxygen consumption (leading to heat production) was modeled in a simple two-state fashion: constant at maximal metabolic rate during the daytime, and constant at routine metabolic rate at night-time. In spite of this simple all-or-none arrangement, our model reproduced the recorded body temperature data very well. The all-or-none shunting mechanism was previously suggested by Malte et al. (Malte et al., 2007). We may seem less justified in simplifying the modeled diurnal metabolism to a two-state oxygen consumption rate. However, analysis of the data of Fish 241 revealed similar velocities of ascents and descents with a gradual increase in swimming speed towards mid-point depth followed by a gradual decrease (Malte et al., 2007). Holland and Sibert (Holland and Sibert, 1993) made similar assumptions. Moreover, there was only a minor difference [$<8\%$ (Malte et al., 2007)] between cooling and heating rates in a lumped parameter model when oxygen consumption was held constant, or when oxygen consumption was varied with vertical swimming speed during vertical excursions. Even though a simple all-or-none mode of regulation explains the present data well a more finely graded regulation can certainly not be excluded. Testing and comparing different modes of regulation would require more detailed knowledge of activity (not only vertical swimming velocity) and temperature data of better spatial and temporal resolution than are available today.

The cooling and heating rate constants found in the lumped parameter model during the vertical excursions were in the range $0.02\text{--}0.04\text{ min}^{-1}$ and $0.2\text{--}0.6\text{ min}^{-1}$, respectively. When we estimated these from the modeled body temperature, we arrived at similar rates (data not shown). Therefore, the present model shows that these cooling and heating rate constants can indeed be the result of an all-or-none shunting mechanism (e.g. diverting blood from the lateral heat exchangers to the dorsal aorta/post-cardinal vein and *vice versa*).

The time-dependent model predicted the recorded T_b very well for various fish on different days. However, in a few fish the metabolic heat production in the white muscle had to be multiplied by a factor of two to yield results that resembled the observed data. This may be because of significant anaerobic metabolism under certain conditions. Tuna white muscle is known to have a large anaerobic capacity with high glycogen stores and extraordinarily high lactate dehydrogenase activity (Hulbert et al., 1979; Arthur et al., 1992; Dickson, 1995). The model only takes aerobic heat production into account and ignores heat production associated with anaerobic glycolysis thus missing the actual scope of white muscle heat production. Increasing white muscle heat production would imply a corresponding decrease in the necessary efficiency of the countercurrent heat exchanger in the blood supply to the white muscle. However, this would only be temporary and, even then, modeling of all realistic scenarios still demonstrated the necessity of a white muscle rete efficiency of around 95%.

Effects of body mass

Scaling the model tuna makes it apparent that body mass is a major contributor to elevated body temperature, thus supporting the similar findings of Malte and colleagues (Malte et al., 2007). Assuming $T_w=20^\circ\text{C}$, a constant volume-specific oxygen consumption rate and high rete efficiencies as estimated from the present calculations, our model predicts that very large tuna would overheat. Thus, in this setting, a 400 kg tuna would reach a core body temperature of approximately 40°C . This, like in all endotherms, stresses the importance of a mass-specific metabolic rate that decreases with size. At this point it is difficult to draw specific conclusions with regard to the value of the exponent of the

metabolic rate–body mass relationship of tuna because of the limited size range for which there are data (Korsmeyer and Dewar, 2001). It is clear from Fig. 8, however, that fractional surface heat loss decreases as body size increases and the significance of heat exchanger efficiency in controlling heat loss increases. Thus, a size-dependent heat loss *via* this route could be achieved by a size-dependent diameter of the arterioles and venules comprising the heat exchangers. There may be an indication of this since Stevens and colleagues (Stevens et al., 1974) found the arteriole and venule diameters to be around 40 and 80 μm in the (central) heat exchanger of a 1.9 kg skipjack tuna whereas Carey and Teal (Carey and Teal, 1966) reported values of around 100 and 200 μm in the similarly arranged (lateral) heat exchanger of a 70 kg bigeye tuna. However, such anatomical data are too scarce to allow definitive conclusions to be drawn. Apart from increasing the possible steady-state T_x , a larger body mass also will slow cooling rates and thus decrease the frequency of vertical excursions.

In conclusion, we have shown that an effective vascular countercurrent heat exchanger in the blood supply of both the red and white muscle is a prerequisite for endothermy in tuna. Furthermore, physiological thermoregulation, as expressed by differential cooling and heating rates, can be fully accounted for by shunting of blood either through or around vascular heat exchangers in an all-or-none fashion. Moreover, by adjusting the heat exchanger efficiencies obtained from steady-state modeling of a large bigeye tuna, we were able to predict the temperature variations recorded in a much smaller tuna performing daily vertical excursions. This suggests that the estimated heat exchanger efficiencies are fairly conservative and that the higher body temperatures in larger individuals are primarily due to a lower fractional surface heat loss and a greater thermal inertia.

Suggestions for future research

This study points to the necessity for studies on heat conservation in white muscle. As a first step, it will be necessary to obtain quantitative anatomical data (i.e. vessel diameter and length as well as interspacing of heat exchanger units) in vascular bands and triads serving the white muscle. This will make it possible to model the maximum possible efficiency of most idealized rete arrangements.

APPENDIX

Model development

Eqn A1 is based on a heat balance on an infinitesimal element. That is, the heat generated within a unit volume of tissue, the heat flux (i.e. conduction) in all three coordinate directions, and the change in energy per unit time must balance:

$$q_x + q_y + q_z + q_{\text{gen}} = q_{x+\text{dx}} + q_{y+\text{dy}} + q_{z+\text{dz}} + \frac{\text{d}E}{\text{dt}}, \quad (\text{A1})$$

where q_x , q_y and q_z are the heat fluxes into the unit volume in the x -, y - and z -directions (respectively), q_{gen} is the heat generated per unit time within the unit volume, $q_{x+\text{dx}}$, $q_{y+\text{dy}}$ and $q_{z+\text{dz}}$ are the heat fluxes out of the unit volume in the x -, y - and z -directions (respectively) and $\text{d}E/\text{dt}$ is the rate of change of energy content in the unit volume.

These energy quantities are given as follows:

$$\begin{aligned} q_x &= -K \frac{\text{d}y \text{d}z}{\text{d}x} \frac{\partial T}{\partial x}, \\ q_{x+\text{dx}} &= - \left[K \frac{\partial T}{\partial x} + \frac{\partial}{\partial x} \left(K \frac{\partial T}{\partial x} \right) \text{d}x \right] \text{d}y \text{d}z, \end{aligned} \quad (\text{A2})$$

$$q_y = -K \frac{\partial T}{\partial y},$$

$$q_{y+dy} = - \left[K \frac{\partial T}{\partial y} + \frac{\partial}{\partial y} \left(K \frac{\partial T}{\partial y} \right) dy \right] dx dz, \quad (A3)$$

$$q_z = -K \frac{\partial T}{\partial z},$$

$$q_{z+dz} = - \left[K \frac{\partial T}{\partial z} + \frac{\partial}{\partial z} \left(K \frac{\partial T}{\partial z} \right) dz \right] dx dy, \quad (A4)$$

$$q_{\text{gen}} = \dot{h}_p dx dy dz, \quad (A5)$$

$$\frac{dE}{dt} = \rho c_p dx dy dz \frac{\partial T}{\partial t}, \quad (A6)$$

where K is the thermal conductivity of the material with the units $\text{J s}^{-1} \text{cm}^{-1} \text{C}^{-1}$, T is the temperature as a function of a given position and time, \dot{h}_p is the volume-specific metabolic heat production in $\text{J s}^{-1} \text{cm}^{-3}$, ρ is the density with the units g cm^{-3} and c_p is the specific heat capacity with the units $\text{J g}^{-1} \text{C}^{-1}$.

Inserting Eqns A2–A6 into Eqn A1 yields:

$$\rho c_p \frac{\partial T}{\partial t} = \frac{\partial}{\partial x} \left(K \frac{\partial T}{\partial x} \right) + \frac{\partial}{\partial y} \left(K \frac{\partial T}{\partial y} \right) + \frac{\partial}{\partial z} \left(K \frac{\partial T}{\partial z} \right) + \dot{h}_p. \quad (A7)$$

With the assumption of uniformity in the z -direction, the differential term in the z -direction in Eqn A7 vanishes. We now introduce a non-directional, uniform, convective cooling term. This can be thought of as a uniform blood flow perpendicular to the xy -plane. This convective flow through the tissue is assumed to have a cooling power at any point proportional to the temperature difference between that point and the surrounding water ($T_b - T_w$). Furthermore it is assumed to be modified by the presence of a heat exchanger with a factor $(1-\varepsilon)$ where ε is the heat exchanger efficiency. This leads to:

$$\rho c_p \frac{\partial T}{\partial t} = \frac{\partial}{\partial x} \left(K \frac{\partial T}{\partial x} \right) + \frac{\partial}{\partial y} \left(K \frac{\partial T}{\partial y} \right) + \dot{h}_p + \dot{v}_b \beta_b (T_w - T_b)(1-\varepsilon). \quad (A8)$$

By dividing through with ρc_p (for muscle), and introducing thermal diffusivity $\kappa=K/(\rho c_p)$ and temperature production $\dot{T}_p=\dot{h}_p/(\rho c_p)$ we get:

$$\frac{\partial T}{\partial t} = \frac{\partial}{\partial x} \left(\kappa \frac{\partial T}{\partial x} \right) + \frac{\partial}{\partial y} \left(\kappa \frac{\partial T}{\partial y} \right) + \dot{T}_p + \dot{v}_b \frac{\beta_b}{\beta_m} (T_w - T_b)(1-\varepsilon). \quad (A9)$$

Finally, introducing the gradient (∇) and the divergence ($\nabla \cdot$) operators and defining a rate constant (dimension s^{-1}) for convective cooling $\varphi=\dot{v}_b \beta_b / \beta_m$ we arrive at:

$$\frac{\partial T}{\partial t} = \nabla \cdot (\kappa \nabla T) + \dot{T}_p + \varphi (T_b - T_w)(1-\varepsilon). \quad (A10)$$

This is the second-order partial differential equation at its final edition, which is a key element in the models. For constant thermal diffusivity, the first term on the right-hand side of Eqn A10 reduces to $\kappa \nabla^2 T$ where $\nabla^2 = \nabla \cdot \nabla$ is the Laplace operator. This is the case inside every homogeneous domain but not on its boundaries.

The last term (the convective term) is thus dependent on the difference between T_b and T_w , and the efficiency of the heat exchanger. T_b will be depend on x and y as well as on time [i.e. $T_b=T_b(x,y,t)$], whereas T_w may or may not depend on time but does not depend on x or y . The efficiency takes on values in the interval 0–1 (i.e. a large ε results in a reduced convective loss). In other words, the final partial differential equation (Eqn A10) is an expression for a 3D model modified into a 2D model taking into

account the z -dimension as a uniform convective blood flow perpendicular to the xy -plane.

LIST OF SYMBOLS AND ABBREVIATIONS

c_p	specific heat capacity ($\text{J g}^{-1} \text{C}^{-1}$)
f	shunting fraction
\dot{h}_p	volume-specific heat production ($\text{J s}^{-1} \text{cm}^{-3}$)
K	thermal conductivity ($\text{J s}^{-1} \text{cm}^{-1} \text{C}^{-1}$)
L	fork length
M	body mass
n	normal to the surface
S	O_2 saturation
t	time
T_b	body temperature at a given coordinate (C)
\dot{T}_p	temperature production, i.e. the rate of change in temperature due to heat production (C s^{-1})
T_w	water temperature (C)
T_x	maximal temperature elevation compared with the ambient water (C)
\dot{v}_b	specific blood flow ($\text{cm}^3 \text{blood s}^{-1} \text{cm}^3_{\text{muscle}}$)
$\dot{V}_{\text{O}_2\text{max}}$	maximum oxygen consumption ($\text{mg O}_2 \text{kg}^{-1} \text{h}^{-1}$)
$\dot{V}_{\text{O}_2\text{rest}}$	resting oxygen consumption ($\text{mg O}_2 \text{kg}^{-1} \text{h}^{-1}$)
∇	gradient operator
$\nabla \cdot$	divergence operator
∇^2	Laplace operator
β	heat capacitance coefficient ($\beta=\rho c_p$ in $\text{J cm}^{-3} \text{C}^{-1}$)
ε	heat exchanger efficiency (dimensionless)
κ	thermal diffusivity [$\kappa=K/(\rho c_p)$ in $\text{cm}^2 \text{s}^{-1}$]
ρ	density (g cm^{-3})
φ	convective cooling rate constant [$(\varphi=\dot{v}_b(\beta_{\text{blood}}/\beta_{\text{muscle}})$ in s^{-1})

This work was supported by The Pelagic Fisheries Research Foundation (PFRP) and The Danish Natural Sciences Research Foundation (FNU).

REFERENCES

- Altringham, J. D. and Shadwick, R. E. (2001). Swimming and muscle function. In *Tuna: Physiology, Ecology And Evolution, Fish Physiology*, vol. 19 (ed. B. A. Block and E. D. Stevens), pp. 331-341. San Diego: Academic Press.
- Arthur, P. G., West, T. G., Brill, R. W., Schulte, P. M. and Hochachka, P. W. (1992). Recovery metabolism of skipjack tuna (*Katsuwonus pelamis*) white muscle: Rapid and parallel changes in lactate and phosphocreatine after exercise. *Can. J. Zool.* **70**, 1230-1239.
- Blank, J. M., Morissette, J. M., Landeira-Fernandez, A. M., Blackwell, S. B., Williams, T. D. and Block, B. A. (2004). *In situ* cardiac performance of Pacific bluefin tuna hearts in response to acute temperature change. *J. Exp. Biol.* **207**, 881-890.
- Block, B. A., Finnerty, J. R., Stewart, A. F. R. and Kidd, J. (1993). Evolution of endothermy in fish: mapping physiological traits on a molecular phylogeny. *Science* **260**, 210-214.
- Bonnick, S. L. (2000). *Osteoporosis, The Hand Book*, third edition, 147 pp. Texas: Cooper Square Press.
- Brill, R. W. and Bushnell, P. G. (2001). The cardiovascular system of tunas. In *Tuna: Physiology, Ecology And Evolution, Fish Physiology*, vol. 19 (ed. B. A. Block and E. D. Stevens), pp. 79-120. San Diego: Academic Press.
- Bushnell, P. G. and Brill, R. W. (1991). Responses of swimming skipjack (*Katsuwonus pelamis*) and yellowfin (*Thunnus albacares*) tunas to acute hypoxia and a model of their cardiorespiratory function. *Physiol. Zool.* **64**, 787-811.
- Caltanburg, R., Cohen, J., Conner, S. and Coo, N. (2004). Thermal properties of cancellous bone. *J. Biomed. Mater. Res.* **9**, 169-182.
- Carey, F. G. (1973). Fishes with warm bodies. *Sci. Am.* **228**, 36-44.
- Carey, F. G. and Teal, J. M. (1966). Heat conservation in tuna fish muscle, *Proc. Natl. Acad. Sci. USA* **56**, 1464-1469.
- Carey, F. G., Teal, J. M., Kanwisher, J. W. and Lawson, K. D. (1971). Warm bodied fish. *Am. Zool.* **11**, 135-145.
- Carey, F. G., Teal, J. M., Kanwisher, J. W. and Stevens, E. D. (1984). Bluefin tuna warm their viscera during digestion. *J. Exp. Biol.* **109**, 1-20.
- Cheng, H. M. and Plewes, D. B. (2002). Tissue thermal conductivity by magnetic resonance thermometry and focused ultrasound heating. *J. Magn. Reson. Imaging* **16**, 598-609.
- Dewar, H. and Graham, J. B. (1994). Studies of tropical tuna swimming performance in a large water tunnel, I. Energetics. *J. Exp. Biol.* **192**, 13-31.
- Dewar, H., Graham, J. B. and Brill, R. W. (1994). Studies of tropical tuna swimming performance in a large water tunnel, II. Thermoregulation. *J. Exp. Biol.* **192**, 33-44.
- Dickson, K. A. (1995). Unique adaptations of the metabolic biochemistry of tunas and billfishes for life in the pelagic environment. *Environ. Biol. Fishes* **42**, 65-97.
- Freund, E. V. (1999). Comparisons of metabolic and cardiac performance in scombrid fishes: Insights into the evolution of endothermy. PhD dissertation, Biological Sciences, Stanford University, Stanford, CA.

- Graham, J. B. and Dickson, K. A.** (2000). The evolution of thunniform locomotion and heat conservation in scombrid fishes: new insights based on the morphology of *Allothunnus fallai*. *Zool. J. Linn. Soc. Lond.* **129**, 419-466.
- Graham, J. B. and Dickson, K. A.** (2001). Anatomical and physiological specializations for endothermy. In *Tuna: Physiology, Ecology And Evolution, Fish Physiology*, vol. 19 (ed. B. A. Block and E. D. Stevens), pp. 121-165. San Diego: Academic Press.
- Graham, J. B., Koehrn, F. J. and Dickson, K. A.** (1983). Distribution and relative proportions of red muscle in scombrid fishes: Consequences of body size and relationships to locomotion and endothermy. *Can. J. Zool.* **61**, 2087-2096.
- Gunn, J. and Block, B. A.** (2001). Advances in acoustic, archival and satellite tagging of tunas. In *Tuna: Physiology, Ecology And Evolution, Fish Physiology*, vol. 19 (ed. B. A. Block and E. D. Stevens), pp. 167-224. San Diego: Academic Press.
- Hensel, H. and Bock, K. D.** (1955). Durchblutung und Wärmeleitfähigkeit des menschlichen Muskels. *Phügers Arch.* **260**, 361-367.
- Holland, K. N. and Sibert, J. R.** (1993). Physiological thermoregulation in bigeye tuna, *Thunnus obesus*. *Environ. Biol. Fishes* **40**, 319-327.
- Holman, J. P.** (1989). *Heat Transfer*. Singapore: McGraw-Hill.
- Hulbert, W. C., Guppy, M., Murphy, B. and Hochachka, P. W.** (1979). Metabolic sources of heat and power in tuna muscles. I. Muscle fine structure. *J. Exp. Biol.* **82**, 289-301.
- Katz, S. L., Syme, D. A. and Shadwick, R. E.** (2001). High-speed swimming, Enhanced power in yellowfin tuna. *Nature* **410**, 770-771.
- Korsmeyer, K. E., and Dewar, H.** (2001). Tuna metabolism and energetics. In *Tuna: Physiology, Ecology and Evolution, Fish Physiology*, vol. 19 (ed. B. A. Block and E. D. Stevens), pp. 35-78. San Diego: Academic Press.
- Lowe, T. E., Brill, R. W. and Cousins, K. L.** (2000). Blood oxygen-binding characteristics of bigeye tuna (*Thunnus obesus*), a high-energy-demand teleost that is tolerant to low ambient oxygen. *Mar. Biol.* **136**, 1087-1098.
- Magnuson, J. J. and Weininger, D.** (1978). Estimation of minimum sustained speed and associated body drag of scombrids. In *The Physiological Ecology of Tunas*, Academic Press, New York.
- Malte, H., Larsen, C., Musyl, M. and Brill, R.** (2007). Differential heating and cooling rates in bigeye tuna (*Thunnus obesus*, Lowe): a model of non-steady-state heat exchange. *J. Exp. Biol.* **210**, 2618-2626.
- Mathieu-Costello, O., Agey, P. J., Logemann, R. B., Brill, R. W. and Hochachka, P. W.** (1992). Capillary-fiber geometrical relationships in tuna red muscle. *Can. J. Zool.* **70**, 1218-1229.
- Musyl, M. K., Brill, R. W., Boggs, C. H., Curran, D. S., Kazama, K. K. and Ski, M. P.** (2003). Vertical movements of bigeye tuna (*Thunnus obesus*) associated with islands, buoys, and seamounts near the main Hawaiian Islands from archival tagging data. *Fish. Oceanogr.* **12**, 152-169.
- Ngadi, M. O. and Ikedaiala, J. N.** (1998). Heat transfer properties of chicken-drum muscle. *J. Sci. Food Agric.* **78**, 12-18.
- Sepulveda, C. A., Dickson, K. A. and Graham, J. B.** (2003). Swimming performance studies on the eastern Pacific bonito (*Sarda chiliensis*), a close relative of the tunas (Family scombridae). I. Energetics. *J. Exp. Biol.* **206**, 2739-2748.
- Song, J., Xu, L. X., Lemons, D. E. and Weinbaum, S.** (1999). Microvascular thermal equilibration in rat trapezius muscle. *Ann. Biomed. Eng.* **27**, 56-66.
- Stevens, E. D. and McLeese, J. M.** (1984). Why bluefin tuna have warm tummies: temperature effect on trypsin and chymotrypsin. *Am. J. Physiol.* **246**, 487-494.
- Stevens, E. D., Lam, H. M. and Kendall, J.** (1974). Vascular anatomy of the counter-current heat exchanger of Skipjack Tuna. *J. Exp. Biol.* **61**, 145-153.
- Urbanchek, M. G., Picken, E. B., Kallainen, L. K. and Kuzon, W., Jr** (2001). Specific force deficit in skeletal muscles of old rats is partially explained by the existence of denervated muscle fibers. *J. Gerontol. A Biol. Sci. Med. Sci.* **56**, 292-297.